

Magnetic approaches to study collective three-dimensional cell mechanics in long-term cultures (invited)

Ruogang Zhao, Thomas Boudou, Wei-Gang Wang, Christopher S. Chen, and Daniel H. Reich

Citation: [Journal of Applied Physics](#) **115**, 172616 (2014); doi: 10.1063/1.4870918

View online: <http://dx.doi.org/10.1063/1.4870918>

View Table of Contents: <http://scitation.aip.org/content/aip/journal/jap/115/17?ver=pdfcov>

Published by the [AIP Publishing](#)

Articles you may be interested in

[Microfluidic immunomagnetic cell separation using integrated permanent micromagnets](#)

[Biomechanics](#) **7**, 054115 (2013); 10.1063/1.4825395

[Stability enhancement of an atomic force microscope for long-term force measurement including cantilever modification for whole cell deformation](#)

[Rev. Sci. Instrum.](#) **83**, 093709 (2012); 10.1063/1.4752023

[Microfluidic three-dimensional hydrodynamic flow focusing for the rapid protein concentration analysis](#)

[Biomechanics](#) **6**, 024132 (2012); 10.1063/1.4730332

[Non-positional cell microarray prepared by shape-coded polymeric microboards: A new microarray format for multiplex and high throughput cell-based assays](#)

[Biomechanics](#) **5**, 032001 (2011); 10.1063/1.3608130

[Fabrication of three-dimensional structures for the assessment of cell mechanical interactions within cell monolayers](#)

[J. Vac. Sci. Technol. B](#) **28**, C6K1 (2010); 10.1116/1.3511435



Re-register for Table of Content Alerts

Create a profile.



Sign up today!



Magnetic approaches to study collective three-dimensional cell mechanics in long-term cultures (invited)

Ruogang Zhao,^{1,a),b)} Thomas Boudou,^{2,c)} Wei-Gang Wang,^{1,d)} Christopher S. Chen,^{2,e)} and Daniel H. Reich¹

¹*Department of Physics and Astronomy, The Johns Hopkins University, 3400 North Charles Street, Baltimore, Maryland 21218, USA*

²*Department of Bioengineering, University of Pennsylvania, 510 Skirkanich Hall, 210 South 33rd Street, Philadelphia, Pennsylvania 19104, USA*

(Presented 5 November 2013; received 23 September 2013; accepted 16 October 2013; published online 15 April 2014)

Contractile forces generated by cells and the stiffness of the surrounding extracellular matrix are two central mechanical factors that regulate cell function. To characterize the dynamic evolution of these two mechanical parameters during tissue morphogenesis, we developed a magnetically actuated micro-mechanical testing system in which fibroblast-populated collagen microtissues formed spontaneously in arrays of microwells that each contains a pair of elastomeric microcantilevers. We characterized the magnetic actuation performance of this system and evaluated its capacity to support long-term cell culture. We showed that cells in the microtissues remained viable during prolonged culture periods of up to 15 days, and that the mechanical properties of the microtissues reached and maintained at a stable state after a fast initial increase stage. Together, these findings demonstrate the utility of this microfabricated bio-magneto-mechanical system in extended mechanobiological studies in a physiologically relevant 3D environment. © 2014 AIP Publishing LLC.

[<http://dx.doi.org/10.1063/1.4870918>]

I. INTRODUCTION

Mechanical stresses generated between cells and their surrounding extracellular matrix (ECM) are critical for cell adhesion, cell function, and tissue development. These stresses are modulated both by the contractile forces generated by cells and by the stiffness of the ECM that opposes those forces. For example, it has been found that increases in cell contractility and ECM stiffness promote cell proliferation^{1,2} and assembly of focal adhesions,^{3,4} whereas reduction in cell contractility and ECM stiffness induces cytoskeleton depolymerization³ and apoptosis.^{5,6} Several technical developments have enabled these recent insights into the role of mechanics in biology. These include the advent of two-dimensional (2D) substrates for cell culture that spans a range of physiologic stiffnesses^{3,7} that can be used to apply force to cells, and whose deformations can be used to report cellular forces.^{8–11} However, despite their utility, these tools are not well suited to address the broader field of tissue remodeling and morphogenesis because the complex reorganization and deformations that occur in 3D are not captured in these 2D settings.

Recently, we introduced an approach that uses elastomeric cantilevers embedded within a 3D collagen microgel

to quantify forces during cell-mediated contraction of the collagen matrix into an aligned microtissue band as a simple model to begin to understand the mechanics of tissue contraction and formation.¹² Furthermore, by integrating these microdevices with a magnetic actuation system, we were able to apply external loading to individual microtissues.¹³ Magneto-mechanical actuation has been used as an effective method to introduce mechanical stimulation to single cells in studies of mechanotransduction.^{11,14–19} The extension of this technique to microtissues in the current study enables simultaneous measurement of both the contractile force and the tissue stiffness. Using this integrated magnetic microtissue tester (MMT) system, we decoupled the cell and ECM contributions to the contraction force and the stiffness of microtissues subjected to short culture periods (up to three days). While these studies demonstrated the MMT's utility as a mechanobiological diagnostic system, for many mechano-sensitive cell types, such as cardiomyocytes and osteocytes, it has been shown that they require relatively long culture periods (weeks) to interact with the surrounding mechanical environment and to reach maturity.²⁰ Therefore, if the MMT system is to be used as a research tool that can accommodate various mechano-sensitive cell types, its long-term culture capacity needs to be evaluated.

In the current study, we present characterization and analysis of the performance of the magnetic actuation system in the MMTs and describe the results of long-term microtissue growth studies. Specifically, we cultured fibroblast populated collagen microtissues in MMT devices for up to 15 days and examined the changes in cell viability as well as the tissues' mechanical properties during this culture period. We showed that cells in the microtissues maintained viability

^{a)}Present address: Department of Biomedical Engineering, University at Buffalo, Buffalo, New York 14260, USA.

^{b)}Author to whom correspondence should be addressed. Electronic mail: rgzhao@buffalo.edu.

^{c)}Present address: Laboratory of Materials and Physical Engineering, Grenoble Institute of Technology, Grenoble 38016, France.

^{d)}Present address: Department of Physics, University of Arizona, Tucson, Arizona 85721, USA.

^{e)}Present address: Department of Biomedical Engineering, Boston University, Boston, Massachusetts 02215, USA.

during this prolonged culture period and that the mechanical properties of the microtissues reached and maintained a stable state after a fast initial increase. Through these examinations, we demonstrated the feasibility of utilizing our system to perform extended mechanobiological studies in a physiologically relevant 3D environment. As such, this microfabricated bio-magneto-mechanical system opens a new window to mechanobiological studies in 3D.

II. MATERIALS AND METHODS

A. Fabrication of magnetic microtissue devices

MMTs were fabricated based on recently developed poly(dimethylsiloxane) (PDMS, Sylgard 184, Dow-Corning) microtissue gauges.^{12,21} They consisted of pairs of flexible pillars that have length $115\ \mu\text{m}$ and cross section $140\ \mu\text{m} \times 35\ \mu\text{m}$ in their flexible sections, separated by $500\ \mu\text{m}$ in $800\ \mu\text{m} \times 400\ \mu\text{m} \times 170\ \mu\text{m}$ deep wells cast in PDMS (Fig. 1(c)). Arrays (10×13) of MMTs (Fig. 1(b)) were fabricated in P35 culture dishes (Fig. 1(a)) via replica molding from molds made by two-layer microlithography, as previously described.¹³ The PDMS used had elastic modulus $1.6\ \text{MPa}$, which yielded pillars with effective spring constant $k = 0.90\ \mu\text{N}/\mu\text{m}$ for small deflections. A nickel sphere with $\sim 100\ \mu\text{m}$ diameter was selected through visual screening

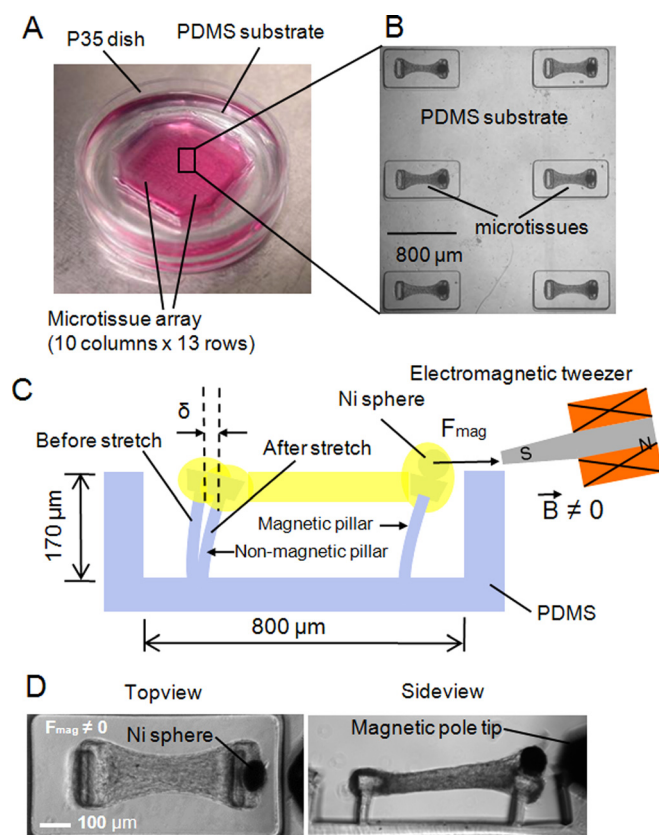


FIG. 1. MMT system and magnetic actuation. (A) Arrays of PDMS microwells were encased in a P35 petri-dish. (B) Microtissues formed in individual microwells. (C) Schematic side-view of a microtissue being stretched by a MMT. A magnetic force (F_{mag}) generated by an applied magnetic field \mathbf{B} drives the movement of the Ni sphere. (D) Representative images show a microtissue under the effect of magnetic force ($F_{\text{mag}} \neq 0$).

from a group of nickel spheres with nominal diameter ranging from $74\ \mu\text{m}$ to $116\ \mu\text{m}$ (CAS 7440-02-0, $-150+200$ mesh, Alfa Aesar), and was adhered to one pillar in each MMT. Fluorescent latex microbeads $1\ \mu\text{m}$ in diameter (L3030, Sigma) were attached on top of the other (non-magnetic) pillar in each well to assist in displacement tracking.

B. Magnetic characterization and actuation

To determine their magnetization curves, representative single nickel spheres were encased in $0.1\ \text{ml}$ of epoxy (Araldite 502) and measured at room temperature with a vector vibrating sample magnetometer (VSM) (DMS Model 10; ADE Technologies, Westwood, MA) (Fig. 2(a)). Actuation of individual magnetic pillars was achieved by applying a ramped magnetic field using a custom-made micromanipulator-controlled electromagnetic tweezer with a sharpened pole tip, which could be brought in close proximity to the Ni sphere (Fig. 1(c)). This system was based on one half of a dual-pole magnetic tweezer system described previously.¹⁹ The tweezer's magnetic field was calibrated with a multi-layer magnetic tunnel junction (MTJ) magnetic field sensor based on a CoFeB/MgO/CoFeB structure²² with an active circular area $7\ \mu\text{m}$ in diameter, defined by photolithography and ion beam etching. For magnetic pillar actuation, changes in the magnetic field and image acquisition were synchronized under computer control.

C. Microtissue seeding and culture

A suspension of NIH 3T3 fibroblasts and $2.5\ \text{mg/ml}$ unpolymerized rat tail collagen type I (BD Biosciences) was introduced into the wells as previously described.¹² Cell culture was maintained up to 15 days in high glucose Dulbecco's Modified Eagle's Medium (DMEM) containing 10% bovine serum, 100 units/ml penicillin, and 100 $\mu\text{g/ml}$ streptomycin (all from Invitrogen). Fibroblast viability was determined by fluorescent labeling of live cells with calcein AM and of dead cells with ethidium homodimer-1 (EthD-1) (Invitrogen) up to 12 days (Fig. 3).

D. Microtissue contraction force and stiffness measurement

The microtissues were immersed in cell culture media and were maintained at $37\ ^\circ\text{C}$ during mechanical testing. The spontaneous contraction force $F' = k\delta'$ generated by a microtissue was determined from the average deflection δ' of the two pillars in the MMT, as previously described.¹³ To stretch a microtissue, the pole tip of the electromagnetic tweezer was immersed in the culture media and brought close to the edge of the MMT well (Figs. 1(c) and 1(d)), and a step-wise ramped magnetic field was applied to pull the magnetic pillar gradually towards the pole tip. A fluorescent image of the microbeads on top of the non-magnetic pillar and a phase contrast image of the microtissue were recorded at every loading step. The increasing tensile force $F = k\delta$ on the microtissue was determined from the deflection δ of the non-magnetic pillar (Fig. 3(a)), which was measured by tracking the movement of the fluorescent microbeads in sequential

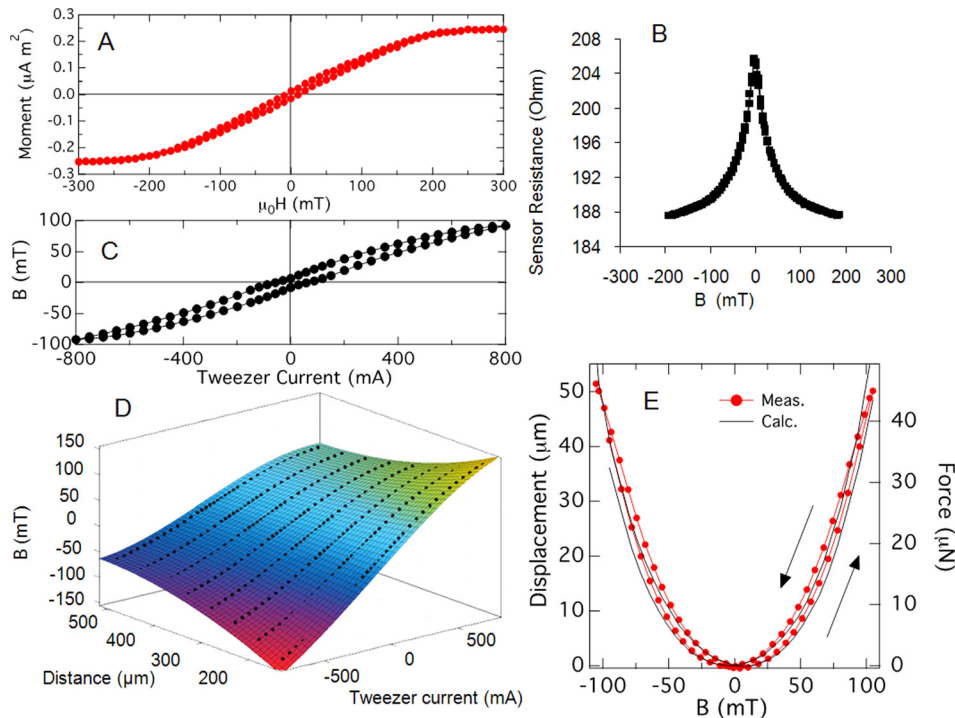


FIG. 2. Magnetic characterization. (A) Typical magnetic moment versus magnetic field for a single Ni sphere. (B) Calibration curve of a microfabricated MTJ sensor used to measure the magnetic tweezers' field. (C) Tweezer magnetic field vs current at a distance of 300 μm from tweezers tip. (D) Surface plot of magnetic field versus tweezers current and tweezers - sample distance, showing bottom branch of hysteresis loop only. (E) Experimentally measured micropillar displacement vs tweezers magnetic field (red solid circles). Force as determined from pillar spring constant $k = 0.9 \mu\text{N}/\mu\text{m}$ may be read from right-hand axis. Black curves show the magnetic force as calculated from the data in panels A and C.

fluorescence images using the SpotTracker plug-in in ImageJ (NIH). The nominal cross sectional area $A_n = dt$ of the center of each microtissue was obtained by measuring the width d from top views prior to stretching, and the thickness t from side views obtained by sectioning the array after completion of stretching experiments. This nominal cross sectional area was then converted to actual area by multiplying a conversion factor determined from confocal imaging of the detailed shape of representative microtissues. During stretching, the cross-sectional area change was minimal and the stress and strain were relatively uniform in this region. Thus, in our analysis the central region of the microtissue was assumed to be under static uniaxial tension. The engineering stress of the microtissue was calculated as $\sigma = F/A$. The strain over the central region of the microtissue was determined based on the sequential phase contrast images obtained during stretching, using a texture correlation image analysis algorithm.²³ Finally, the tensile elastic modulus of the central region was taken as the slope of the engineering stress-engineering strain curve (Fig. 3(c)).

E. Microscopy

To measure the contractile force and to track the pillar bending and microtissue deformation during tensile testing, individual MMTs were imaged on a Nikon TE2000-E motorized microscope with a Plan-Fluor 10X objective using a CoolSNAP-HQ camera (Photometrics, Tucson, AZ). Samples were maintained at 37 °C during live cell imaging.

III. RESULTS

To assess the performance of the magnetic actuation in the MMT system, and to validate the accuracy of our force measurements, we measured the magnetic properties of the magnetic components of the system, and measured the force

generation on the magnetic pillars in MMTs without microtissues present. Figure 2(a) shows the magnetic moment of a representative Ni sphere, as measured via VSM. The Ni spheres are ferromagnetic but have small remanent magnet moments, approximately 6% of their saturation moment. The magnetic moments $\mu(\mathbf{B})$ of these spheres were thus approximately linear with applied magnetic field \mathbf{B} over the ~ 150 mT field range used in our experiments, albeit with some small hysteresis.

As determination of the magnetic force requires knowledge of both the magnetic field and the field gradient acting on the Ni spheres, we carried out a detailed calibration of the electromagnetic tweezers' field profile, using a MTJ sensor. For these measurements, the pole tip of the tweezers was placed at fixed distances ranging from 100 μm to 500 μm from the sensor and the current was cycled between -0.8 A and 0.8 A while recording the electrical resistance of the MTJ sensor. The resistance was then converted to magnetic field based on the calibration curve of the MTJ sensor (Fig. 2(b)). The tweezers' magnetic field is shown at a distance of 300 μm from the tip (Fig. 2(c)), and as a surface plot as a function of both the tweezers current and the distance between the pole tip and the sensor (Fig. 2(d)). To characterize the actuation of the magnetic pillars when no tissue was attached, the pole tip of the tweezers was placed at a fixed location relative to the microwell edge and the magnetic field was cycled between -105 mT and 105 mT while imaging the top of the magnetic pillar to record its position. Figure 2(e) shows such data recorded at an initial tweezers-sphere separation of 350 μm . As the tweezers' field \mathbf{B} magnetized the Ni sphere, the approximately quadratic behavior is consistent with the expectation for the magnetic force on a dipole $\mu(\mathbf{B})$ in an inhomogeneous field, $\mathbf{F}_{\text{Mag}} = \nabla(\mu(\mathbf{B}) \cdot \mathbf{B})$. To validate the accuracy of the magnetic field calibration of the tweezers, the gradient of the magnetic field was calculated

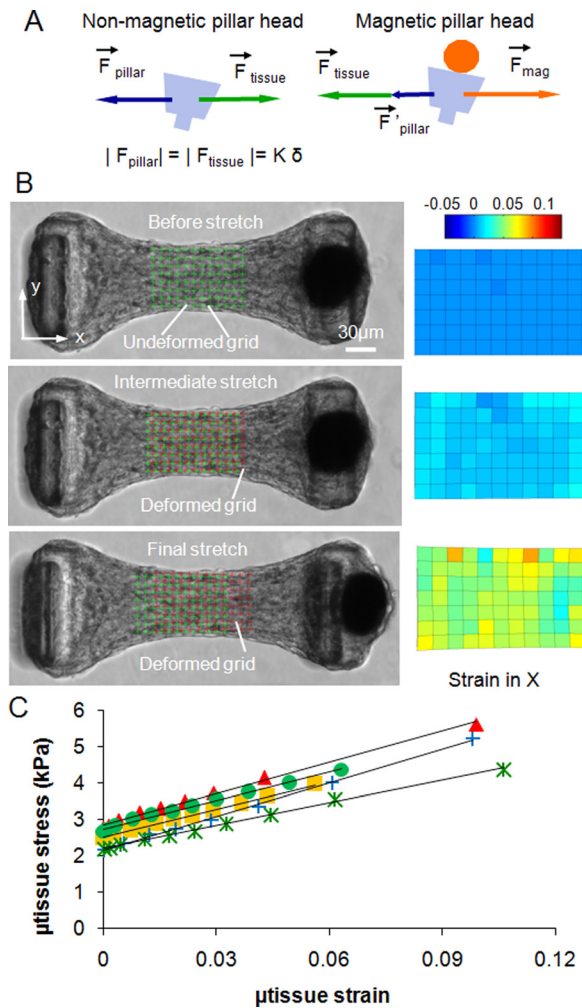


FIG. 3. Microtissue stiffness determination. (A) Free body diagrams showing the force balance on the pillar heads when a microtissue was stretched. The increased tensile force F_{tissue} in the microtissue due to external loading was reported by the increased bending δ of the non-magnetic pillar. (B) Representative images show the grid of nodes used in the texture correlation algorithm and the corresponding X-direction strain maps before, during and at the end of the stretch. (C) Sample stress-strain curves of microtissues after 2 days in culture.

based on the surface plot (Fig. 2(d)) and was used to calculate the magnetic force acting on the Ni sphere from the above expression for F_{Mag} . In this computation, the changes in the field and field gradient due to the changes in the position of the bead were taken into account. As shown in Fig. 2(e), this agrees quite well with the force as determined by the deflection of the PDMS pillar. At shorter tip-sphere separations, this system was capable of producing magnetic forces up to $\sim 110 \mu$ N.

When suspensions of 3T3 fibroblasts and unpolymerized type-I collagen were centrifuged into the wells and the collagen was polymerized, the cells contracted the collagen matrix, leading on the timescale of hours to the formation of dog-bone shaped microtissue constructs wrapped around the pillar heads, and suspended between the pillars in a highly aligned band (Fig. 1(b)). The contractile tension within the microtissues deflected the pillars, causing displacements of the pillar heads observable via optical microscopy.¹² Consistent with our previous studies,^{24–26} we did not observe

adverse effects on cells cultured in the presence of the Ni spheres.

We used the MMTs to perform quasi-static tensile tests on microtissues to examine their stiffness. We displaced the magnetic pillar at a constant strain rate of approximately 0.09%/s in a step-wise ramp, up to total strains of typically 9%. Three images of a microtissue at strains of 0%, 1.6%, and 6.2% are shown in Fig. 3(b). (Note that these strains were measured relative to the initial pre-stressed state achieved during the tissues' self-assembly and compaction around the pillars.) As shown in Fig. 3(a), the displacement of the magnetic pillar is driven by the balance of three forces: the magnetic force in the Ni sphere, the force of the microtissue, and the restoring "spring" force of the pillar itself. In contrast, the position of the non-magnetic pillar is determined solely by the balance between the microtissue's force and the pillar's spring force. Thus, the deflection δ of the non-magnetic pillar measures the tissue's force, and in particular its deflection from its zero-field position yields a direct read-out of the force applied during the magnetic stretching. This force increased with the field applied to the magnetic pillar and reached up to 15–30 μ N depending on the stiffness of the tissues. We note in particular that this method to measure the tissue force renders our technique insensitive to variations in the magnetic force that may arise from the $\sim 10\%$ variability in the diameter of the Ni spheres or variation in the placement of the tweezer tip. The stress of the microtissues was calculated by dividing the tensile force by the cross-sectional area as detailed in the Methods section, and the strain distribution in the central region of the microtissue was determined by a texture correlation algorithm,²³ wherein the motion of features in the microtissue images was tracked over the grid shown superimposed on the phase contrast images in Fig. 3(b). We found the strain distribution was relatively uniform (Fig. 3(b)), and so reported the average strain over the measured region. The resulting stress-strain curves were linear, as seen in Fig. 3(c), which shows a set of data obtained for several different microtissues after 2 day's culture. The tissues' elastic moduli were reported as the slope of these curves.

We next characterized the cell viability and the evolution of stiffness and contractility in our microtissues during long-term culture in the MMT device. We measured the cell viability, tissue contractile force, tissue elastic modulus, cross-sectional area, and cell number in microtissues up to 15 days after seeding. We found the cells were predominantly viable (Live, Fig. 4(a)) with the percentage of cells that were dead (Dead, Fig. 4(a)) and attached to the microtissue always remaining below 5% through a 12 day culture period (Fig. 4(c)). This is consistent with a relatively constant cell number per microtissue during the same culture period (Fig. 4(b)). We observed a dog-bone shaped microtissue forming between the two pillars within several hours after seeding and a rapid increase in the tissue contractile force during the first 3 days after seeding (Figs. 5(a) and 5(b)), as has been reported previously.¹² This increase in contractile force was accompanied by an increase in tissue elastic modulus (Fig. 5(c)) and decrease in tissue cross sectional area (Fig. 5(d)). Beyond 3 days, the microtissues remained relatively stable

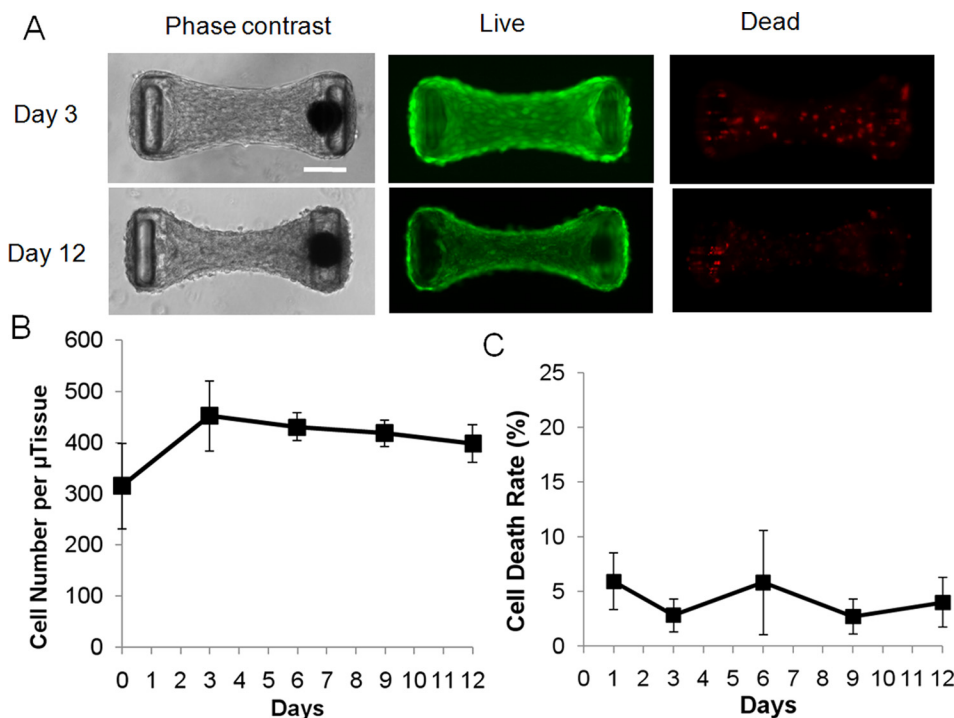


FIG. 4. Cells are mostly viable throughout the 12-day culture period. (A) Representative images of day 3 and day 12 microtissues. Live cells were fluorescently labeled with calcein AM (green) and dead cells were labeled with ethidium homodimer-1 (EthD-1, red). (B) Cell number per tissue. (C) The percentage of dead cells that were still attached to the microtissue during tissue maturation. Sample size: $N > 5$. Scale bar = $100 \mu\text{m}$. All data are presented as Mean \pm S.D.

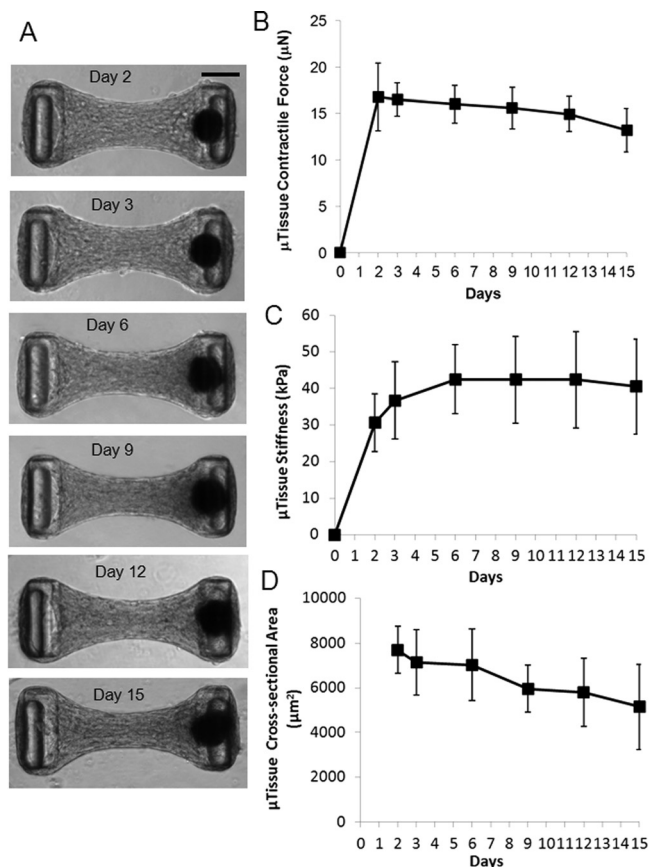


FIG. 5. Microtissues gained rapid maturation over a several days culture period and then remained stable for up to 15 days. Phase contrast images (A), contractile force (B), elastic modulus (C) and cross-sectional area (D) of fibroblast populated collagen microtissues during a 15 day culture period. Sample size: $N > 6$. All data are presented as Mean \pm S.D.

with tissue contraction force and cross-sectional area decreasing slightly through day 15. Interestingly, the tissue elastic modulus continued to rise and reached a plateau only after day 6, indicating a lag in the development of tissue stiffness as compared to tissue contraction force. After day 6, the tissue stiffness remained stable with only a slight decrease at day 15 (Fig. 5(c)).

IV. DISCUSSION AND CONCLUSION

While much work has demonstrated that many biological functions can be regulated by cell contractility or ECM stiffness,^{3,27,28} there has been little work examining these two mechanical parameters simultaneously²⁹ in the context of 3D tissue remodeling. Most previous mechanobiology studies are based on 2D culture models that do not support the major structural rearrangements that typically occur during tissue morphogenesis.^{7,30} For example, studies demonstrating a role for substrate stiffness in many cellular functions^{3,27,28} rely on pre-setting stiffness of the substrate before cell seeding. Although some dynamic remodeling of the underlying surface occurs,^{28,31} significant restructuring of the matrix is inherently limited. Here, we developed a new magnetic tool to measure and manipulate the mechanics of cell-mediated collagen contraction and alignment, and verified and calibrated the performance of its magnetic components. Our system allows for the evolution of tissue mechanical properties, while also measuring these properties. Our microfabricated, magnetically driven mechanical testing system combines the advantages of generating large arrays of microtissues with the ability to study single microtissues in detail, and thus enables relatively high-throughput examination of the microtissues' mechanical properties for a full range of conditions. Since the microtissues anchor themselves to the cantilevers during their self assembly, our

system allows in-situ testing without the perturbations to these delicate microscale specimens that would arise from transferring them to conventional mechanical testing systems, in which loading of specimens is laborious and a major source of variability.^{32,33} Through prolonged culture, we further demonstrated the feasibility of using this system for long-term mechanobiological studies. Collectively, our system offers advantages over existing approaches by providing a novel window into the mechanics of tissue remodeling in real time.

ACKNOWLEDGMENTS

This work was supported in part by National Institutes of Health Grant No. HL90747. VSM measurements and MTJ fabrication used facilities maintained by the Johns Hopkins Materials Research Science and Engineering Center.

- ¹N. A. Hasaneen, S. Zucker, J. Cao, C. Chiarelli, R. Panettieri, and H. Foda, *FASEB J.* **19**, 1507–1509 (2005).
- ²T. A. Ulrich, E. de Juan Pardo, and S. Kumar, *Cancer Res.* **69**, 4167–4174 (2009).
- ³T. Yeung, P. C. Georges, L. A. Flanagan, B. Marg, M. Ortiz, M. Funaki, N. Zahir, W. Ming, V. Weaver, and P. A. Janmey, *Cell Motil. Cytoskeleton* **60**, 24–34 (2005).
- ⁴B. Hinz, V. Dugina, C. Ballestrem, B. Wehrle-Haller, and C. Chaponnier, *Mol. Biol. Cell* **14**, 2508–2519 (2003).
- ⁵H. B. Wang, M. Dembo, and Y. L. Wang, *Am. J. Physiol. Cell Physiol.* **279**, c1345–c1350 (2000).
- ⁶S. Niland, A. Cremer, J. Fluck, J. A. Eble, T. Krieg, and S. Sollberg, *J. Invest. Dermatol.* **116**, 686–692 (2001).
- ⁷W. H. Guo, M. T. Frey, N. A. Burnham, and Y. L. Wang, *Biophys. J.* **90**, 2213–2220 (2006).
- ⁸M. E. Wall, P. S. Weinhold, T. Siu, T. D. Brown, and A. J. Banes, *J. Biomech.* **40**, 173–181 (2007).
- ⁹J. L. Tan, J. Tien, D. Pirone, D. S. Gray, and C. S. Chen, *Proc. Natl. Acad. Sci. U. S. A.* **100**, 1484–1489 (2003).
- ¹⁰X. Trepap, M. R. Wasserman, T. E. Angelini, E. Millet, D. A. Weitz, J. P. Butler, and J. J. Fredberg, *Nat. Phys.* **5**, 426–430 (2009).
- ¹¹N. J. Sniadecki, A. Anguelouch, M. T. Yang, C. M. Lamb, Z. Liu, S. B. Kirschner, Y. Liu, D. H. Reich, and C. S. Chen, *Proc. Natl. Acad. Sci. U. S. A.* **104**, 14553–14558 (2007).
- ¹²W. R. Legant, A. Pathak, M. T. Yang, V. S. Deshpande, R. M. McMeeking, and C. S. Chen, *Proc. Natl. Acad. Sci. U. S. A.* **106**, 10097–10102 (2009).
- ¹³R. Zhao, T. Boudou, W. Wang, C. S. Chen, and D. H. Reich, *Adv. Mater.* **25**, 1699–1705 (2013).
- ¹⁴N. Wang, J. P. Butler, and D. E. Ingber, *Science* **260**, 1124–1127 (1993).
- ¹⁵B. D. Matthews, D. A. LaVan, D. R. Overby, J. Karavitis, and D. E. Ingber, *Appl. Phys. Lett.* **85**, 2968 (2004).
- ¹⁶J. Dobson, *Nat. Nanotechnol.* **3**, 139–143 (2008).
- ¹⁷R. J. Mannix, S. Kumar, F. Cassiola, M. Montoya-Zavala, E. Feinstein, M. Prentiss, and D. E. Ingber, *Nat. Nanotechnol.* **3**, 36–40 (2008).
- ¹⁸B. Hu, A. J. E. Haj, and J. Dobson, *Int. J. Mol. Sci.* **14**, 19276–19293 (2013).
- ¹⁹Y.-C. Lin, C. M. Kramer, C. S. Chen, and D. H. Reich, *Nanotechnology* **23**, 075101 (2012).
- ²⁰M. Guvendiren and J. A. Burdick, *Nat. Commun.* **3**, 792 (2012).
- ²¹T. Boudou, W. R. Legant, A. Mu, M. Borochin, N. Thavandiran, M. Radisic, P. Zandstra, J. Epstein, K. Margulies, and C. S. Chen, *Tissue Eng. Part A* **18**, 910–919 (2012).
- ²²W. G. Wang, S. Hageman, M. G. Li, S. X. Huang, X. M. Kou, X. Fan, J. Q. Xiao, and C. L. Chien, *Appl. Phys. Lett.* **99**, 102502 (2011).
- ²³R. Zhao and C. A. Simmons, *J. Biomech.* **45**, 76–82 (2012).
- ²⁴A. Hultgren, M. Tanase, C. S. Chen, G. J. Meyer, and D. H. Reich, *J. Appl. Phys.* **93**, 7554–7556 (2003).
- ²⁵A. Hultgren, M. Tanase, E. J. Felton, K. Bhadriraju, A. K. Salem, C. S. Chen, and D. H. Reich, *Biotechnol. Prog.* **21**, 509–515 (2005).
- ²⁶M. Tanase, E. J. Felton, D. S. Gray, A. Hultgren, C. S. Chen, and D. H. Reich, *Lab Chip* **5**, 569–696 (2005).
- ²⁷N. D. Leipzig and M. S. Shoichet, *Biomaterials* **30**, 6867–6878 (2009).
- ²⁸D. E. Discher, P. Janmey, and Y.-l. Wang, *Science* **310**, 1139–1143 (2005).
- ²⁹D. Karamichos, R. A. Brown, and V. Mudera, *J. Biomed. Mater. Res. A* **83A**, 887–894 (2007).
- ³⁰C. Y. Yip, J.-H. Chen, R. Zhao, and C. A. Simmons, *Arterioscler. Thromb. Vasc. Biol.* **29**, 936–942 (2009).
- ³¹C. S. Chen, *J. Cell Sci.* **121**, 3285–3292 (2008).
- ³²S. C. Schutte, Z. Chen, K. G. Brockbank, and R. M. Nerem, *Tissue Eng. Part A* **16**, 3149–3157 (2010).
- ³³T. Wakatsuki, M. S. Kolodney, G. I. Zahalak, and E. L. Elson, *Biophys. J.* **79**, 2353–2368 (2000).